物理化学学报(*Wuli Huaxue Xuebao*)
March *Acta Phys. -Chim. Sin.* **2014,** *30* (3), 527–534 527

[Article] doi: 10.3866/PKU.WHXB201401072 www.whxb.pku.edu.cn

Cs取代对Ni-$H_3PW_{12}O_{40}/SiO_2$催化剂结构性质和催化性能的影响

金 浩[1,2,*] 孙晓丹[1] 董 澍[3] 吴义志[3] 孙素华[1] 刘 杰[1]
朱慧红[1] 杨 光[1] 伊晓东[2,*] 方维平[2]

([1]中国石油化工股份有限公司抚顺石油化工研究院, 辽宁 抚顺 113001; [2]厦门大学化学化工学院, 固体表面物理化学国家重点实验室, 醇醚酯化工清洁生产国家工程实验室, 福建 厦门 361005; [3]中国石油抚顺石化公司石油二厂, 辽宁 抚顺 113004)

摘要: 采用两步浸渍法和载体上的原位反应制备了一系列Cs部分取代的Ni-$Cs_xH_{3-x}PW_{12}O_{40}/SiO_2$催化剂, 并用$N_2$吸附比表面积测定(BET)、电感耦合等离子体发射光谱(ICP)、X射线衍射(XRD)、拉曼光谱(Raman)、原位X射线衍射(*in situ* XRD)、NH_3程序升温脱附(NH_3-TPD)、H_2程序升温还原(H_2-TPR)、H_2程序升温脱附(H_2-TPD)、吡啶吸附傅里叶变换红外(FTIR)光谱等分析测试技术对催化剂进行了表征. 以正癸烷为模型化合物, 对催化剂的加氢裂化性能进行了评价. 结果表明, 8%Ni-50%$Cs_{1.5}H_{1.5}PW/SiO_2$催化剂具有最高的C_{5+}收率, 明显优于8% Ni-50%H_3PW/SiO_2催化剂和工业催化剂. 随着Cs在$Cs_xH_{3-x}PW$中比例的增加, 正癸烷的转化率逐渐降低, 而C_{5+}选择性则逐渐提高. 当催化剂具有合适的孔径时, 选择性的提高是由于催化剂酸性的减弱, 而转化率的降低则是由于催化剂加氢能力的减弱.

关键词: 加氢裂化; 正癸烷; 双功能催化剂; Ni; Cs; $H_3PW_{12}O_{40}$
中图分类号: O643

Influence of Cs Substitution on the Structural Properties and Catalytic Performance of Ni-$H_3PW_{12}O_{40}/SiO_2$ Catalysts

JIN Hao[1,2,*] SUN Xiao-Dan[1] DONG Shu[3] WU Yi-Zhi[3] SUN Su-Hua[1] LIU Jie[1]
ZHU Hui-Hong[1] YANG Guang[1] YI Xiao-Dong[2,*] FANG Wei-Ping[2]

([1]*Fushun Research Institute of Petroleum and Petrochemicals, SINOPEC, Fushun 113001, Liaoning Province, P. R. China*; [2]*State Key Laboratory for Physical Chemistry of the Solid Surfaces, National Engineering Laboratory for Green Chemical Productions of Alcohols, Ethers and Esters, College of Chemistry and Chemical Engineering, Xiamen University, Xiamen 361005, Fujian Province, P. R. China*; [3]*PetroChina Fushun Petrochemical Company No.2 Refinery, Fushun 113004, Liaoning Province, P. R. China*)

Abstract: Cs-substituted Ni-$Cs_xH_{3-x}PW_{12}O_{40}/SiO_2$ catalysts were prepared by two-step impregnation and *in situ* reaction on the support. The catalysts were characterized by N_2 adsorption measurements, inductively coupled plasma atomic emission spectrometry, Raman spectroscopy, *in situ* X-ray diffraction, NH_3-temperature programmed desorption (TPD), H_2-temperature programmed reduction, H_2-TPD, and Fourier transform infrared spectroscopy. The hydrocracking of *n*-decane was used to study the catalytic performance of the Ni-$Cs_xH_{3-x}PW_{12}O_{40}/SiO_2$ catalysts. The highest C_{5+} yield obtained for 8%Ni-50%$Cs_{1.5}H_{1.5}PW/SiO_2$ was superior to those of 8%Ni-50% H_3PW/SiO_2 and an industrial catalyst. The conversion of *n*-decane slightly decreased and the C_{5+} selectivity increased with increasing Cs content in the $Cs_xH_{3-x}PW$ catalysts. Ni-$Cs_xH_{3-x}PW_{12}O_{40}/SiO_2$ catalysts possessed

Received: October 8, 2013; Revised: January 6, 2014; Published on Web: January 7, 2014.
*Corresponding authors. JIN Hao, Email: jinhao.fshy@sinopec.com; Tel: +86-24-56389744.
YI Xiao-Dong, Email: xdyi@xmu.edu.cn; Tel/Fax: +86-592-2186291.
The project was supported by the National Key Basic Research Program of China (973) (2010CB226903), National Natural Science Foundation of China (21073147, 21303140), and Program for Changjiang Scholars and Innovative Research Team in University, China (IRT1036).
国家重点基础研究发展规划项目 (973) (2010CB226903), 国家自然科学基金(21073147, 21303140)和教育部长江学者和创新团队发展计划项目(IRT1036)资助

relatively large pore sizes, so the improved selectivity might have been due to a weaker acidity of the catalysts. The reduced conversion might have been due to a weaker hydrogenation ability.

Key Words: Hydrocracking; *n*-Decane; Bifunctional catalyst; Ni; Cs; $H_3PW_{12}O_{40}$

1 Introduction

Hydrocracking is a catalytic petroleum refining process that is commonly applied to convert the heavier petroleum fractions such as vacuum distillates into gasoline or middle distillates.[1,2] As the growing demand for high quality middle distillates and more stringent specifications, hydrocracking becomes a strategic process in a modern refinery.[3]

Hydrocracking catalysts are bifunctional, i.e., the acid sites which provide the cracking function and metal sites with a hydrogenation-dehydrogenation function.[4–7] The typical acidic supports are amorphous oxides, mixtures of oxides, zeolites, and silicoaluminaphosphates. The metals most commonly used are Pt, Pd or bimetallic systems (i.e., NiW, NiMo, and CoMo). The balance between the acidity of the support-concentration of acidic sites and their strength-hydro/dehydrogenation activity of the metal is of primary importance in determining the selectivity of hydroisomerization and distribution of cracking products.

Heteropolyacids (HPAs) with Keggin structure and their salts have been widely investigated as catalysts in many oxidation and acid-catalyzed reactions due to their strong acidity, high oxidation potential, and redox character.[8–12] The tungstophosphoric acid ($H_3PW_{12}O_{40}$) (HPW) is among the most extensively studied,[13–15] since it possesses the highest Brønsted acidity. Nevertheless, the main drawback of such materials for catalytic application is their low specific surface area (<10 $m^2 \cdot g^{-1}$). Therefore, for many catalytic applications, they are usually impregnated on different porous materials with high surface area. Among these carriers, silica has been widely favored as the supporting material for HPA, since it interacts weakly with the Keggin anions and thus preserves their structure.[16,17] Yet in reactions that involve polar media, true heterogenization of $H_3PW_{12}O_{40}$ could not be achieved on silica, and the acid leached out into the reaction mixture.[18,19]

Heteropolyacid salts are prepared by exchanging part of the protons of HPA with cations with higher ionic radii, like Cs^+ and NH_4^+.[20,21] They have higher surface area (up to 150 $m^2 \cdot g^{-1}$ compared to 10 $m^2 \cdot g^{-1}$ of HPA) and improved thermal stability than their parent acids. In addition, they are known to be insoluble even in liquids as polar as water. Consequently, HPA salts should be better suited for practical applications that might involve polar reagents in harsh operating conditions. However, these salts tend to form colloidal suspensions in polar media, resulting in difficulties in the catalyst separation.[22] Moreover, their small particle size (unit in μm) limits their application for use as catalysts in commercial fixed bed or slurry type reactors.[23]

An obvious solution as often applied in industrial practice is to support these HPA salts on a larger particle size (unit in mm) carrier. Unfortunately, the insolubility of HPA salts with big cation makes conventional aqueous impregnation on different supports impossible. Consequently, the catalysts were prepared by sequential impregnation and *in situ* reaction on different types of supports, as reported in previous literature.[24–28]

In our previous work,[16] we reported that non-sulfided supported Ni-$H_3PW_{12}O_{40}/SiO_2$ catalysts exhibited high hydrocracking activity of *n*-decane. But $H_3PW_{12}O_{40}$ has an excessive acidity and an overhigh cracking activity, which increases the probability to undergo secondary reactions. We also studied hydrogen spillover on Ni-$Cs_xH_{3-x}PW_{12}O_{40}$ (x=0, 1, 2) double-function hydrocracking catalysts by temperature programmed desorption and thermodynamics calculation.[29] The results show that the hydrogen adsorption amount on the two-component Ni-$Cs_xH_{3-x}PW_{12}O_{40}$ (x=0, 1, 2) catalysts is much greater than that on single-component catalysts, such as nickel, tungstophosphoric acid, and its cesium salts. Moreover, the Cs salts of $H_3PW_{12}O_{40}$ overcome these disadvantages, which have a more widely tunable acidity, a higher thermal stability, and much lower water solubility.[21]

Recently, we[30] also reported that non-sulfided supported Ni-$Cs_xH_{3-x}PW_{12}O_{40}/SiO_2$ catalysts prepared by direct synthesis using tetraethyl orthosilicate as SiO_2 source. Taking into account the thermal stability of $Cs_xH_{3-x}PW_{12}O_{40}$ and the strong interaction between $Cs_xH_{3-x}PW_{12}O_{40}$ and support by direct synthesis, the calcination temperature of the catalyst could not be too high. The properties of support were restricted by calcination temperature and the pore size of the support was about 4 nm.

In the present paper, the Ni-$Cs_xH_{3-x}PW_{12}O_{40}/SiO_2$ catalysts were prepared by two-step impregnation and *in situ* reaction on the SiO_2 support. It avoided the restriction of support properties due to calcination temperature and the strong interaction between $Cs_xH_{3-x}PW_{12}O_{40}$ and support by direct synthesis. The catalysts were characterized by N_2 adsorption (BET), inductively coupled plasma atomic emission spectrometry (ICP), X-ray diffraction (XRD), Raman, *in situ* XRD, NH_3-temperature programmed desorption (NH_3-TPD), H_2-temperature programmed reduction (H_2-TPR), H_2-TPD, and Fourier transform infrared (FTIR) spectra of pyridine adsorption. The influence of Cs substitution on catalytic performance of the catalysts for hydrocracking of *n*-decane was investigated.

2 Experimental

2.1 Preparation of catalysts

The catalysts were prepared by two-step impregnation and *in*

situ reaction on the SiO_2 support. Typical procedures for the preparation of Ni-$Cs_xH_{3-x}PW_{12}O_{40}/SiO_2$ catalysts are as follows: SiO_2 support (Qingdao Haiyang Chemical Co., specific surface area (378 $m^2 \cdot g^{-1}$), 40–60 mesh) was impregnated with a solution containing the desired quantities of $Ni(NO_3)_2$ (Shanghai Hengxin Chemical Reagent Co., analyzed grade) and Cs_2CO_3 (Sinopharm Chemical Reagent Co., 3N). Impregnated samples were dried overnight at 110 °C and then calcined in air at 400 °C for 3 h. Then the samples were impregnated with a solution containing the desired quantities of $H_3PW_{12}O_{40}$ (Sinopharm Chemical Reagent Co., analyzed grade). After impregnation, samples were dried overnight at 110 °C without calcination.

Samples prepared with 8% amount of nickel and 50% amount of $Cs_xH_{3-x}PW_{12}O_{40}$ were labeled as 8%Ni-50%$Cs_xH_{3-x}PW/SiO_2$, wherein "*x*" stands for the molar of replaced by Cs in the $Cs_xH_{3-x}PW_{12}O_{40}$ (x=0–3), while $Cs_xH_{3-x}PW$ stands for the $Cs_xH_{3-x}PW_{12}O_{40}$.

2.2 Characterization

The chemical composition of the samples was determined using an IRIS Intrepid II XSP ICP atomic emission spectrometer (Thermo, USA).

The surface area (BET) and pore volume of the catalysts were determined by means of nitrogen adsorption at –196 °C on an adsorption automatic instrument (Micromeritics Tristar 3020, USA). The samples were pretreated at 300 °C for 3 h in a vacuum.

Powder X-ray diffraction (XRD) characterization was carried out on a Panalytical (NetherLands) X2 Pert PRO automatic powder diffractometer operated at 40 kV and 30 mA, using Cu K_α (λ=0.15406 nm) monochromatized radiation in all cases. Each step of 0.0167° was measured for 10 s from 10° to 90° (2θ). JCPDS file database was used for peak identification.

Raman spectra were recorded with a Renishaw (UK) inVia Raman System equipped with a charge-coupled device (CCD) detector at room temperature. The 532 nm of diode laser was used as the exciting source with a power of 22 mW.

In situ XRD was performed under the 5%H_2/Ar mixture atmosphere. The first spectrum was recorded at room temperature (25 °C). The temperature was then raised up to 300, 350, 400, 450, 500, 550, 600, 650, 700, 750, and 800 °C, maintained at each value for 0.5 h before recording a new spectrum.

Acid properties were determined by ammonia temperature-programmed desorption in a Micromeritics AutoChem II 2920 analyzer (USA). 0.2 g of catalyst sample was filled in a U-shaped quartz reactor tube and a thermocouple was placed onto the top of the sample. All samples were pretreated in Ar (20 mL·min^{-1}) at 400 °C for 2 h then in H_2 (20 mL·min^{-1}) for 1 h. After cooling down to 100 °C, 10%NH_3/Ar was passed over the samples for 30 min. Then, the samples were swept with Ar for 60 min and finally the desorption step was performed from 100 to 700 °C at a heating rate of 10 °C·min^{-1} and 30 mL·min^{-1} of Ar total flow. The desorbed products were monitored by thermal conductivity detector (TCD) and mass spectrometry (MS) equipment simultaneously.

The H_2-temperature programmed reduction experiments were performed with a gas chromatography (GC)-TPR apparatus. The samples (50 mg) were treated in a flow of Ar (20 mL·min^{-1}) at 300 °C for 30 min and then cooled to 50 °C. The samples were subsequently switched to a flow of 5%H_2/Ar mixture (20 mL·min^{-1}) and heated from 50 to 900 °C at a rate of 10 °C·min^{-1}. The effluent gas mixture was passed through a cold trap at 0 °C to remove water. Hydrogen consumption was monitored by an on-line gas chromatograph equipped with a TCD.

H_2-TPD measurements were done in a Micromeritics AutoChem II 2920 analyzer. 0.2 g of catalyst sample was filled in a U-shaped quartz reactor tube and a thermocouple was placed onto the top of the sample. All samples were pretreated in Ar (20 mL·min^{-1}) at 400 °C for 2 h then in H_2 (20 mL·min^{-1}) for 1 h. After cooling down to 50 °C, the samples were swept with Ar for 60 min and finally the desorption step was performed from 50 to 700 °C at a heating rate of 10 °C·min^{-1} and 30 mL·min^{-1} of Ar total flow.

FTIR spectra of pyridine adsorption were recorded using a Thermo Nicolet Nexus spectrometer equipped with a liquid-nitrogen-cooled mercury cadmium telluride (MCT) detector. The samples were pressed into self-supporting wafers and treated in H_2 at 400 °C in an IR cell for 1 h followed by evacuation at 400 °C for 5 min to remove the gas phase H_2. After cooling to 100 °C, the samples were exposed to pyridine vapor for 10 min. Then the spectra were recorded after evacuation at high temperatures. The IR spectra were recorded in the spectral range of 1700 to 1400 cm^{-1} with 32 scans and at a resolution of 4 cm^{-1}.

2.3 Catalytic studies

n-Decane used in the present study was purchased from Tianjin Kermel Chemical Reagent Co. (analyzed Grade) without further purification.

The catalytic performance of the catalysts was measured in a down flow fixed-bed quartz tube reactor cased in a stainless steel tube (inner diameter (id)=8 mm; 50 cm in length) at 2.0 MPa, T=300 °C, liquid hourly space velocity (LHSV)=2.92 h^{-1} and H_2/*n*-decane volume ratio of 1500. Prior to reaction, all the catalysts were reduced by a flow of H_2 at 400 °C for 1 h. 0.5 g of the catalyst was used in each experiment. *n*-Decane was introduced into the reactor using a micro pump (2ZB-1L10). The products were collected and identified when the reaction had begun for 4 h. The activity data were usually obtained after 10 h reaction. The products were directly analyzed on-line in a gas chromatograph with an OV-101 capillary column (30 m) and flame ionization detector (FID).

For comparison, an industrial hydrocracking catalyst FC-16 (NiW/USY zeolite) was also measured for hydrocracking of *n*-decane under the same conditions. The industrial catalyst was obtained from FuShun Research Institute of petroleum and petrochemicals, SINOPEC.

3 Results and discussion

3.1 Catalysts characterization

The structural information, pore size distribution, and composition of the catalysts are presented in Table 1 and Table 2. The determined chemical composition from ICP is as expected, indicating that the results of chemical analysis of the catalysts are in good agreement with desired stoichiometries for Ni and $Cs_xH_{3-x}PW$. It can be observed that the surface area and pore volume of SiO_2 after supporting Ni and $Cs_xH_{3-x}PW$ decrease remarkably, while the pore size increases slightly. This may be due to Ni and $Cs_xH_{3-x}PW$ blocking the micropores of the SiO_2 support, therefore, the surface area and pore volume decrease, the pore size increases slightly. However, the surface area and pore volume of the 8%Ni-50%$Cs_xH_{3-x}PW/SiO_2$ catalysts increase with increasing the proportion of Cs in $Cs_xH_{3-x}PW$. This may be due to the much higher surface area of $Cs_xH_{3-x}PW$ with increasing proportion of Cs in $Cs_xH_{3-x}PW$, which makes the surface area of the catalysts become higher.

The XRD patterns of 8%Ni-50%$Cs_xH_{3-x}PW/SiO_2$ and $Cs_xH_{3-x}PW$ catalysts are presented in Fig.1. It is clear that the intensity of the diffraction peaks of the 8%Ni-50%$Cs_xH_{3-x}PW/SiO_2$ catalysts decreased compared to the $Cs_xH_{3-x}PW$ due to the interaction of $Cs_xH_{3-x}PW$ with Ni species and SiO_2 support. The 8%Ni-50%H_3PW/SiO_2 catalyst shows the presence of characteristic peaks of NiO (37.0°, 43.1°, and 62.6°) and Keggin structure of H_3PW.[27] It is interesting to notice that the diffraction peaks of the Keggin structure of $Cs_xH_{3-x}PW$ (18.2°, 23.7°, 25.9°, 29.9°, 35.4°, 43.2°, 54.3°, and 62.2°) appeared and the intensities of these peaks increased with increasing the proportion of Cs in $Cs_xH_{3-x}PW$ on the catalysts. This could be attributed to the interaction of $Cs_xH_{3-x}PW$ with Ni species and SiO_2 support.

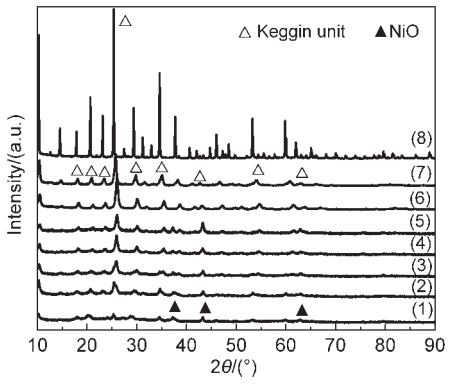

Fig.1 XRD patterns of 8%Ni-50%$Cs_xH_{3-x}PW/SiO_2$ catalysts

(1) 8%Ni-50%H_3PW/SiO_2, (2) 8%Ni-50%$Cs_{0.5}H_{2.5}PW/SiO_2$, (3) 8%Ni-50%CsH_2PW/SiO_2, (4) 8%Ni-50%$Cs_{1.5}H_{1.5}PW/SiO_2$, (5) 8%Ni-50%Cs_2HPW/SiO_2, (6) Cs_2HPW, (7) CsH_2PW, (8) H_3PW

The Raman spectra of the 8%Ni-50%$Cs_xH_{3-x}PW/SiO_2$ catalysts are presented in Fig.2. Raman scattering spectroscopy is an effective method to study the structure of the supported $Cs_xH_{3-x}PW$ because it is extremely sensitive to the Keggin unit, and the support has no significant interference on the Raman signals originating from the Keggin unit. All the 8%Ni-50%$Cs_xH_{3-x}PW/SiO_2$ catalysts display similar Raman spectra. The sharp and intense peak at 1009 cm^{-1} can be assigned to stretching vibrations of P—O bond of P—O_4, whereas peaks at lower wavenumbers can be assigned to W=O (990 cm^{-1}) and W—O—W (905 cm^{-1}) stretching vibrations.[31,32] The strong interaction between H_3PW and SiO_2 support reduces the symmetry of Keggin unit. Furthermore, it can be speculated that the intro-

Table 1 Chemical composition and textural information of the catalysts

Catalyst	Composition*						$S_{BET}/(m^2\cdot g^{-1})$	Pore volume/$(cm^3\cdot g^{-1})$	Pore size/nm
	Theoretical/%			ICP/%					
	Ni	Cs	W	Ni	Cs	W			
SiO_2	–	–	–	–	–	–	378	1.1	10.0
8%Ni-50%H_3PW/SiO_2	8	0	38.3	7.92	0	37.6	123	0.29	10.2
8%Ni-50%$Cs_{0.5}H_{2.5}PW/SiO_2$	8	1.13	37.4	7.88	1.08	36.5	125	0.32	10.3
8%Ni-50%CsH_2PW/SiO_2	8	2.21	36.6	7.90	2.15	35.7	132	0.35	10.5
8%Ni-50%$Cs_{1.5}H_{1.5}PW/SiO_2$	8	3.24	35.8	7.93	3.16	35.0	139	0.37	10.8
8%Ni-50%Cs_2HPW/SiO_2	8	4.23	35.1	7.89	4.15	34.4	176	0.41	11.1
industrial catalyst	–	–	–	–	–	–	227	0.31	5.5

* mass fraction

Table 2 Pore size distribution of the catalysts

Catalyst	Pore size distribution/% *			
	<5 nm	5–10 nm	10–20 nm	20–50 nm
SiO_2	2.29	35.27	61.82	0.62
8%Ni-50%H_3PW/SiO_2	0	37.21	62.56	0.23
8%Ni-50%$Cs_{0.5}H_{2.5}PW/SiO_2$	0	35.26	64.46	0.28
8%Ni-50%CsH_2PW/SiO_2	0	33.10	66.54	0.36
8%Ni-50%$Cs_{1.5}H_{1.5}PW/SiO_2$	0	31.56	68.07	0.37
8%Ni-50%Cs_2HPW/SiO_2	0	28.91	70.64	0.42

* volume fraction

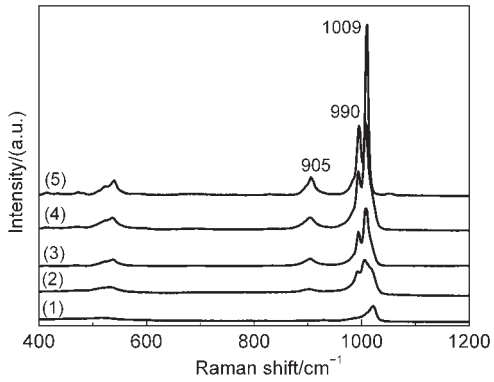

Fig.2 Raman spectra of 8%Ni-50%$Cs_xH_{3-x}PW/SiO_2$ catalysts

(1) 8%Ni-50%H_3PW/SiO_2, (2) 8%Ni-50%$Cs_{0.5}H_{2.5}PW/SiO_2$, (3) 8%Ni-50%CsH_2PW/SiO_2, (4) 8%Ni-50%$Cs_{1.5}H_{1.5}PW/SiO_2$, (5) 8%Ni-50%Cs_2HPW/SiO_2

duction of Cs also will weaken the interaction between $Cs_xH_{3-x}PW$ and the SiO_2 support becomes weaker, reducing the influence on Keggin unit′s symmetry. Therefore, the intensity of these peaks increases with increasing the proportion of Cs in $Cs_xH_{3-x}PW$ on the catalysts. The Raman results are consistent with XRD characterization.

The thermal stabilities of 8%Ni-50%$Cs_{1.5}H_{1.5}PW/SiO_2$ and 8%Ni-50%H_3PW/SiO_2 catalysts under the hydrogen atmosphere were studied by *in situ* XRD and the patterns are shown in Fig.3. When the temperature is lower than 500 °C, the XRD patterns of the 8%Ni-50%$Cs_{1.5}H_{1.5}PW/SiO_2$ catalyst only present the characteristic peaks of the Keggin structure. Compared with the XRD pattern of the catalyst at 25 °C, the characteristic diffraction peaks of the catalyst calcined at higher temperature have no change. In the XRD patterns of the catalyst calcined at temperature higher than 500 °C, the new intense diffraction peaks of $H_{0.5}WO_3$ (23.5°, 34°) and $Cs_{0.3}WO_3$ (44°) are observed. While for the 8%Ni-50%H_3PW/SiO_2 catalyst calcined at 500 °C, the new intense diffraction peak of $H_{0.5}WO_3$ (23.5°) is observed. The 8%Ni-50%$Cs_{1.5}H_{1.5}PW/SiO_2$ catalyst has improved thermal stability than 8%Ni-50%H_3PW/SiO_2 catalyst. These results indicate that $Cs_{1.5}H_{1.5}PW$ decomposes when the calcination temperature exceeds 500 °C.

The acidity of the 8%Ni-50%$Cs_xH_{3-x}PW/SiO_2$ catalysts was

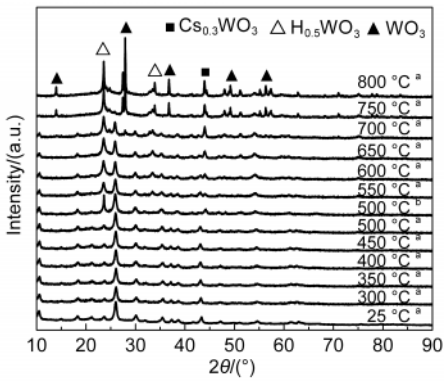

Fig.3 *In situ* XRD patterns of the catalysts calcined at different temperatures under the 5% H_2/Ar mixture atmosphere

^{a}8%Ni-50%$Cs_{1.5}H_{1.5}PW/SiO_2$, ^{b}8%Ni-50%H_3PW/SiO_2

characterized by NH_3-TPD and the FTIR of pyridine adsorption. The NH_3-TPD profiles of the 8%Ni-50%$Cs_xH_{3-x}PW/SiO_2$ catalysts are shown in Fig.4. All the catalysts show two desorption peaks of ammonia near 170 and 540 °C, respectively. It is evident from Fig.4 that the amount of NH_3 desorbed of the catalysts decreases with increasing the proportion of Cs in $Cs_xH_{3-x}PW$.

In other words, the acid amount of the catalysts decreases with decreasing the H^+ content in $Cs_xH_{3-x}PW$ on the catalysts. The 8%Ni-50%$Cs_xH_{3-x}PW/SiO_2$ catalysts show relatively higher acidity compared to the industrial catalyst.

The FTIR spectra of pyridine adsorbed on reduced 8%Ni-50%$Cs_xH_{3-x}PW/SiO_2$ catalysts are shown in Fig.5. The use of IR spectroscopy to detect the adsorbed pyridine enables to distinguish different acid sites. The band at 1446 cm^{-1} is due to the pyridine adsorbed on the Lewis acid sites. On the other hand, the band at 1538 cm^{-1} is due to the pyridine adsorbed on the Brønsted acid sites. The band at 1488 cm^{-1} is due to the contributions of Lewis and Brønsted acid sites.[33,34] The characteristic absorption bands of pyridine adsorbed on Lewis acid sites and Brønsted acid sites were observed for 8%Ni-50%

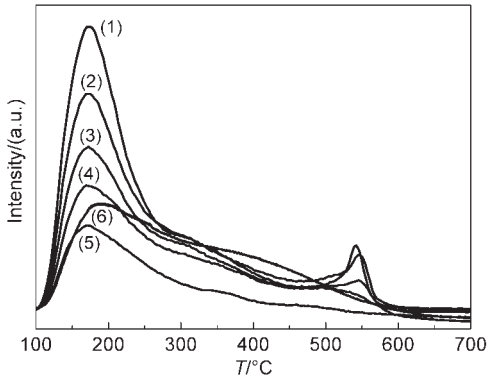

Fig.4 NH_3-TPD profiles of reduced catalysts

(1) 8%Ni-50%H_3PW/SiO_2, (2) 8%Ni-50%$Cs_{0.5}H_{2.5}PW/SiO_2$, (3) 8%Ni-50%CsH_2PW/SiO_2, (4) 8%Ni-50%$Cs_{1.5}H_{1.5}PW/SiO_2$, (5) 8%Ni-50%Cs_2HPW/SiO_2, (6) industrial catalyst

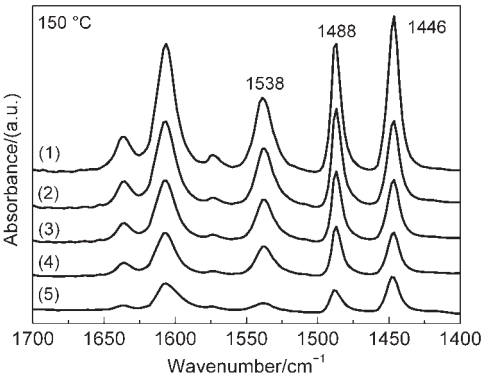

Fig.5 FTIR spectra of pyridine adsorbed and desorbed on reduced catalysts

(1) 8%Ni-50%H_3PW/SiO_2, (2) 8%Ni-50%$Cs_{0.5}H_{2.5}PW/SiO_2$, (3) 8%Ni-50%CsH_2PW/SiO_2, (4) 8%Ni-50%$Cs_{1.5}H_{1.5}PW/SiO_2$, (5) 8%Ni-50%Cs_2HPW/SiO_2

$Cs_xH_{3-x}PW/SiO_2$ catalysts. The IR results show that the intensities of absorption bands for Brønsted acid sites (1538 cm^{-1}) and Lewis acid sites (1446 cm^{-1}) decrease with increasing the proportion of Cs in $Cs_xH_{3-x}PW$, and relative amount of Lewis acid sites is higher than that of Brønsted acid sites. The results are consistent with NH_3-TPD characterization.

The H_2-TPR profiles of the 8%Ni-50%$Cs_xH_{3-x}PW/SiO_2$ catalysts are shown in Fig.6. The 8%Ni-50%H_3PW/SiO_2 catalyst displays three reduction peaks. The first reduction peak near 400 °C corresponds to the reduction of NiO species, which had weak interaction with the H_3PW. The *in situ* XRD results showed that the $Cs_xH_{3-x}PW$ begins to decompose when the calcinations temperature exceeds 500 °C. The second reduction peak near 580 °C is mainly attributed to the reduction of NiO species, which had strong interaction with the W species of the catalysts. The third reduction peak near 700 °C corresponds to the reduction of W species. However, the 8%Ni-50%$Cs_xH_{3-x}PW/SiO_2$ (x=0.5, 1, 1.5, 2) catalysts show two reduction peaks. The first reduction peak near 400 °C corresponds to the reduction of NiO species and the peak area becomes larger. The second reduction peak near 690 °C corresponds to the reduction of W species. This may be due to the interaction between NiO and $Cs_xH_{3-x}PW$ gradually weakened with increasing the proportion of Cs in $Cs_xH_{3-x}PW$. The reduction peak (580 °C) shifts to lower temperature (400 °C) and the peak area (around 400 °C) becomes larger. The phenomenon is consistent with the result of Raman characterization.

The H_2-TPD profiles of the 8%Ni-50%$Cs_xH_{3-x}PW/SiO_2$ catalysts are shown in Fig.7. All the catalysts present two H_2-desorbed peaks near 160 and 450 °C, respectively. The amount of H_2 desorbed decreases with increasing the proportion of Cs in $Cs_xH_{3-x}PW$. In other words, the amount of H_2 desorbed increases with increasing content of H^+ in the $Cs_xH_{3-x}PW$ on the catalysts.

This phenomenon may be explained by the hydrogen spillover, which has been found in our past work.[16,17,27,35] The dissociated hydrogen molecule on the metal Ni can spill to the acid sites ($Cs_xH_{3-x}PW$) and combine with the H^+. Both the dissociated molecule hydrogen and the H^+ of the $Cs_xH_{3-x}PW$ are highly reactive hydrogen species, which will produce the relatively stable species H_n^+. It seems that there is a balance on the surface of the $Cs_xH_{3-x}PW$, that is

$$H_n^+ \overset{K}{\rightleftharpoons} H^+ + (n-1)H\cdot$$

As the concentration of H_n^+ species on the surface of $Cs_xH_{3-x}PW$ increases, the reactive hydrogen species $H\cdot$ can reversely spill over back to the Ni^0 sites. This process can form a reactive hydrogen species layer covering the catalyst's surface. The $Cs_xH_{3-x}PW$ can not only act as the acid sites but also act as the hydro-dehydrogenation sites. This is a non-classical bifunctional mechanism which was reported in some papers.[16,27,35,36]

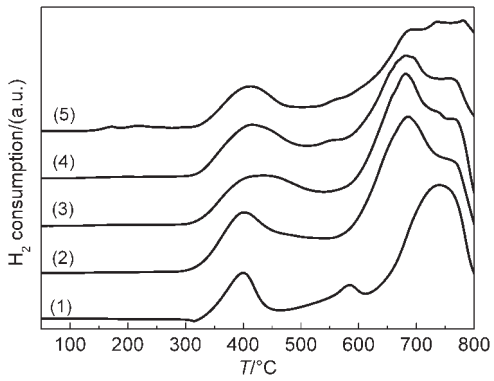

Fig.6 H_2-TPR profiles of the catalysts

(1) 8%Ni-50%H_3PW/SiO_2, (2) 8%Ni-50%$Cs_{0.5}H_{2.5}PW/SiO_2$, (3) 8%Ni-50%CsH_2PW/SiO_2, (4) 8%Ni-50%$Cs_{1.5}H_{1.5}PW/SiO_2$, (5) 8%Ni-50%Cs_2HPW/SiO_2

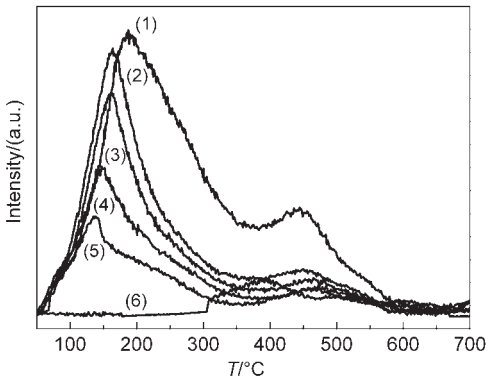

Fig.7 H_2-TPD profiles of the catalysts

(1) 8%Ni-50%H_3PW/SiO_2, (2) 8%Ni-50%$Cs_{0.5}H_{2.5}PW/SiO_2$, (3) 8%Ni-50%CsH_2PW/SiO_2, (4) 8%Ni-50%$Cs_{1.5}H_{1.5}PW/SiO_2$, (5) 8%Ni-50%Cs_2HPW/SiO_2, (6) industrial catalyst

3.2 Catalytic activity

The activity of the 8%Ni-50%$Cs_xH_{3-x}PW/SiO_2$ catalysts for hydrocracking of *n*-decane is shown in Table 3, wherein the conversion of *n*-decane and the C_5^+ selectivity were taken to express the activity of the catalyst. The catalytic performance of the prepared catalysts was compared with that of a typical NiW/zeolite industrial catalyst. It is evident from Table 3 that the 8%Ni-50%$Cs_xH_{3-x}PW/SiO_2$ catalysts and the industrial catalyst all exhibit high activity for the hydrocracking of *n*-decane. Among the catalysts tested, 8%Ni-50%H_3PW/SiO_2 catalyst shows highest conversion of *n*-decane and lower C_{5+} selectivity. Moreover, after the introduction of Cs species, the conversion of *n*-decane decreases while the C_{5+} selectivity is improved for 8%Ni-50%$Cs_xH_{3-x}PW/SiO_2$ catalysts. Furthermore, the 8%Ni-50%$Cs_xH_{3-x}PW/SiO_2$ catalysts show higher activity compared to the industrial catalyst.

With increasing the proportion of Cs in $Cs_xH_{3-x}PW$, the conversion of *n*-decane decreases from 99.2% to 89.5% for 8%Ni-50%$Cs_xH_{3-x}PW/SiO_2$ catalysts. The reduced 8%Ni-50%H_3PW/SiO_2 catalyst shows the highest activity, superior to the 8%Ni-50%$Cs_xH_{3-x}PW/SiO_2$ ($x\neq0$) catalyst and the industrial catalyst. Combined with the results of H_2-TPD and H_2-TPR characterization, it can be inferred that the hydrogenation ability of the catalysts is gradually weakened with increasing the proportion of Cs in $Cs_xH_{3-x}PW$.

With increasing the proportion of Cs in $Cs_xH_{3-x}PW$, the C_{5+}

Table 3 Catalytic performance of the catalysts for *n*-decane hydrocracking

Catalyst	Conversion/%	C_{5+} selectivity/%	C_{5+} yield/%
8%Ni-50%H_3PW/SiO_2	99.2	74.1	73.5
8%Ni-50%$Cs_{0.5}H_{2.5}PW/SiO_2$	97.9	76.5	74.9
8%Ni-50%CsH_2PW/SiO_2	96.3	79.4	76.5
8%Ni-50%$Cs_{1.5}H_{1.5}PW/SiO_2$	95.8	83.8	80.3
8%Ni-50%Cs_2HPW/SiO_2	89.5	85.2	76.2
industrial catalyst	87.5	71.0	62.1

reaction conditions: T=300 °C; $v(H_2)/v$(*n*-decane)=1500; p=2 MPa, and liquid hourly space velocity (LHSV)=2.92 h^{-1}. The activity data were obtained after 10 h reaction.

selectivity of the catalysts increases from 74.1% to 85.2%. The reduced 8%Ni-50%Cs_2HPW/SiO_2 shows the highest C_{5+} selectivity, superior to the 8%Ni-50%H_3PW/SiO_2 catalyst and the industrial catalyst. Based on the results of NH_3-TPD and FTIR spectra of pyridine adsorption, it can be concluded that the acidity of the 8%Ni-50%$Cs_xH_{3-x}PW/SiO_2$ catalysts is in line with their C_{5+} selectivity, which is ascribed to the gradually lower cracking activity of the catalysts with increasing the proportion of Cs in $Cs_xH_{3-x}PW$ owing to their weaker acidity. According to bifunctional reaction scheme,[37] the hydroisomerization and hydrocracking go through the formation of carbonium ions, the lower the acid strength of the acid sites, the lower will be the average lifetime of the carbonium ions on the acid sites. This will decrease the probability to undergo secondary reactions. In addition, the pore size of the 8%Ni-50%$Cs_xH_{3-x}PW/SiO_2$ catalysts increases slightly with increasing the proportion of Cs in $Cs_xH_{3-x}PW$. Indeed, it is well-known that the micropore of zeolite is beneficial for secondary reactions. Therefore, it can be expected that large pore size of the 8%Ni-50%$Cs_xH_{3-x}PW/SiO_2$ catalysts would favor the diffusion of liquid products while decreasing the probability of secondary reactions. Moreover, the 8%Ni-50%$Cs_{1.5}H_{1.5}PW/SiO_2$ catalyst shows the highest C_{5+} yield of 80.3% in the 8%Ni-50%$Cs_xH_{3-x}PW/SiO_2$ catalysts, which is much higher than the yield of 73.5% on the 8%Ni-50%H_3PW/SiO_2 catalyst and the yield of 62.1% on the industrial catalyst.

4 Conclusions

The results obtained in the present work indicate that the 8%Ni-50%$Cs_xH_{3-x}PW/SiO_2$ catalysts′ acidity *via* NH_3-TPD and FTIR spectra of pyridine adsorption, and hydrogenation-dehydrogenation function *via* H_2-TPR and H_2-TPD decrease with Cs gradual substituting in $Cs_xH_{3-x}PW$. The conversion of *n*-decane decreases slightly and the C_{5+} selectivity of the catalysts increases with increasing the proportion of Cs in $Cs_xH_{3-x}PW$. The best result was obtained on the 8%Ni-50%$Cs_{1.5}H_{1.5}PW/SiO_2$ catalyst with the C_{5+} selectivity of 83.8% at the *n*-decane conversion of 95.8%, which is much higher than that of the industrial catalyst.

References

(1) Morawski, I.; Mosio-Mosiewski, J. *Fuel Process. Technol.* **2006,** *87*, 659. doi: 10.1016/j.fuproc.2006.01.006

(2) Ancheyta, J.; Sánchez, S.; Rodríguez, M. A. *Catal. Today* **2005,** *109*, 76. doi: 10.1016/j.cattod.2005.08.015

(3) Roussel, M.; Lemberton, J. L.; Guisnet, M.; Cseri, T.; Benazzi, E. *J. Catal.* **2003,** *218*, 427. doi: 10.1016/S0021-9517(03)00164-7

(4) Calemma, V.; Peratello, S.; Perego, C. *Appl. Catal. A: Gen.* **2000,** *190*, 207. doi: 10.1016/S0926-860X(99)00292-6

(5) Ren, X. T.; Li, N.; Cao, J. Q.; Wang, Z. Y.; Liu, S. Y.; Xiang, S. H. *Appl. Catal. A: Gen.* **2006,** *298*, 144. doi: 10.1016/j.apcata.2005.09.031

(6) Zeng, S. Q.; Blanchard, J.; Breysse, M.; Shi, Y. H.; Su, X. T.; Nie, H. *Appl. Catal. A: Gen.* **2005,** *294*, 59. doi: 10.1016/j.apcata.2005.07.015

(7) Roussel, M.; Norsic, S.; Lemberton, J. L.; Guisnet, M.; Cseri, T.; Benazzi, E. *Appl. Catal. A: Gen.* **2005,** *279*, 53. doi: 10.1016/j.apcata.2004.10.011

(8) Timofeeva, M. N. *Appl. Catal. A: Gen.* **2003,** *256*, 19. doi: 10.1016/S0926-860X(03)00386-7

(9) Zhang, Q. D.; Tan, Y. S.; Yang, C. H.; Han, Y. Z. *J. Mol. Catal. A: Chem.* **2007,** *263*, 149. doi: 10.1016/j.molcata.2006.08.044

(10) Zhang, P.; Huang, M.; Chu, W.; Luo, S. Z.; Li, T. *Acta Phys. -Chim. Sin*. **2013,** *29*, 770. [张 坡, 黄 明, 储 伟, 罗仕忠, 李 通. 物理化学学报, **2013,** *29*, 770.] doi: 10.3866/PKU.WHXB201301152

(11) Gu, L. Y.; Gao, B. J.; Fang, X. L. *Acta Phys. -Chim. Sin*. **2013,** *29*, 191. [顾来沅, 高保娇, 房晓琳. 物理化学学报, **2013,** *29*, 191.] doi: 10.3866/PKU.WHXB201210266

(12) Yuan, C. Y.; Chen, J. *Chin. J. Catal.* **2011,** *32*, 1191. doi: 10.1016/S1872-2067(10)60236-7

(13) Kumar, G. S.; Vishnuvarthan, M.; Palanichamy, M.; Murugesan, V. *J. Mol. Catal. A: Chem.* **2006,** *260*, 49. doi: 10.1016/j.molcata.2006.07.050

(14) Yang, X. K.; Chen, L. F.; Wang, J. A.; Noreña, L. E.; Novaro, O. *Catal. Today* **2009,** *148*, 160. doi: 10.1016/j.cattod.2009.03.022

(15) Wang, J. A.; Chen, L. F.; Noreña, L. E.; Navarrete, J. *Appl. Catal. A: Gen.* **2009,** *357*, 223. doi: 10.1016/j.apcata.2009.01.023

(16) Qiu, B.; Yi, X. D.; Lin, L.; Fang, W. P.; Wan, H. L. *Catal. Today* **2008,** *131*, 464. doi: 10.1016/j.cattod.2007.10.095

(17) Qiu, B.; Yi, X. D.; Lin, L.; Fang, W. P.; Wan, H. L. *Catal. Commun.* **2009,** *10*, 1296. doi: 10.1016/j.catcom.2009.02.007

(18) Vazquez, P.; Pizzio, L.; Romanelli, G.; Autino, J.; Caceres, C.; Blanco, M. *Appl. Catal. A: Gen.* **2002,** *235*, 233, doi: 10.1016/

S0926-860X(02)00266-1

(19) Haber, J.; Pamin, K.; Matachowski, L.; Mucha, D. *Appl. Catal. A: Gen.* **2003,** *256*, 141. doi: 10.1016/S0926-860X(03)00395-8

(20) Narasimharao, K.; Brown, D. R.; Lee, A. F.; Newman, A. D.; Siril, P. F.; Tavener, S. J.; Wilson, K. *J. Catal.* **2007,** *248*, 226. doi: 10.1016/j.jcat.2007.02.016

(21) Luzgin, M. V.; Kazantsev, M. S.; Volkova, G. G.; Wang, W.; Stepanov, A. G. *J. Catal.* **2011,** *277*, 72. doi: 10.1016/j.jcat.2010.10.015

(22) Okuhara, T.; Kimura, M.; Kawai, T.; Xu, Z.; Nakato, T. *Catal. Today* **1998,** *45*, 73. doi: 10.1016/S0920-5861(98)00251-X

(23) Choi, S.; Wang, Y.; Nie, Z.; Liu, J.; Peden, C. H. F. *Catal. Today* **2000,** *55*, 117. doi: 10.1016/S0920-5861(99)00231-X

(24) Soled, S.; Miseo, S.; McVicker, G.; Gates, W. E.; Gutierrez, A.; Paes, J. *Catal. Today* **1997,** *36*, 441. doi: 10.1016/S0920-5861(96)00235-0

(25) Yang, W.; Billy, J.; Taârit, Y. B.; Védrine, J. C.; Essayem, N. *Catal. Today* **2002,** *73*, 153. doi: 10.1016/S0920-5861(01)00508-9

(26) Gao, R. H.; Chen, H.; Le, Y. Y.; Dai, W. L.; Fan, K. N. *Appl. Catal. A: Gen.* **2009,** *352*, 61. doi: 10.1016/j.apcata.2008.09.031

(27) Jin, H.; Yi, X. D.; Sun, S. H.; Liu, J.; Yang, G.; Zhu, H. H.; Fang, W. P. *Fuel Process. Technol.* **2012,** *97*, 52. doi: 10.1016/j.fuproc.2012.01.011

(28) Popa, A.; Sasca, V.; Holclajtner-Antunović, I. *Microporous Mesoporous Mat.* **2012,** *156*, 127. doi: 10.1016/j.micromeso.2012.02.030

(29) Yuan, S. H.; Ji, N. H.; Xia, W. S.; Yi, X. D.; Fang, W. P. *React. Kinet. Mech. Catal.* **2012,** *106*, 475. doi: 10.1007/s11144-012-0448-y

(30) Jin, H.; Guo, D. Y.; Sun, X. D.; Sun, S. H.; Liu, J.; Zhu, H. H.; Yang, G.; Yi, X. D.; Fang, W. P. *Fuel* **2013,** *112*, 134. doi: 10.1016/j.fuel.2013.05.007

(31) Rocchiccioli-Deltcheff, C.; Fournier, M.; Franck, R.; Thouvenot, R. *Inorg. Chem.* **1983,** *22*, 207. doi: 10.1021/ic00144a006

(32) Qu, X. S.; Guo, Y. H.; Hu, C. W. *J. Mol. Catal. A: Chem.* **2007,** *262*, 128. doi: 10.1016/j.molcata.2006.08.026

(33) Chen, L. F.; Noreña, L. E.; Wang, J. A.; Zhou, X. L.; Navarrete, J.; Hernández, I.; Montoya, A.; Pérez Romo, P.; Salas, P.; Castella Pergher, S. *Catal. Today* **2008,** *133–135*, 331.

(34) Varisli, D.; Dogu, T.; Dogu, G. *Ind. Eng. Chem. Res.* **2008,** *47*, 4071. doi: 10.1021/ie800192t

(35) Jin, H.; Yi, X. D.; Sun, X. D.; Qiu, B.; Fang, W. P.; Weng, W. Z.; Wan, H. L. *Fuel* **2010,** *89*, 1953. doi: 10.1016/j.fuel.2009.11.031

(36) Kuba, S.; Lukinskas, P.; Grasselli, R. K.; Gates, B. C.; Knözinger, H. *J. Catal.* **2003,** *216*, 353. doi: 10.1016/S0021-9517(02)00125-2

(37) Corma, A.; Martinez, A.; Pergher, S.; Peratello, S.; Perego, C.; Bellusi, G. *Appl. Catal. A: Gen.* **1997,** *152*, 107. doi: 10.1016/S0926-860X(96)00338-9